PUBLICATIONS OF THE ASTRONOMICAL SOCIETY OF THE PACIFIC, **115**:1388–1406, 2003 December

The Gemini Near-Infrared Imager (NIRI)

KLAUS W. HODAPP,[1] JOSEPH B. JENSEN,[2] EVERETT M. IRWIN,[3] HUBERT YAMADA,[3] RANDOLPH CHUNG,[3] KENT FLETCHER,[3] LOUIS ROBERTSON,[3] JOSEPH L. HORA,[3,4] DOUGLAS A. SIMONS,[2] WENDY MAYS,[2] ROBERT NOLAN,[2] MATTHIEU BEC,[2] MICHAEL MERRILL,[5] AND ALBERT M. FOWLER[5]

Received 2003 June 3; accepted 2003 September 10; published 2003 October 20

ABSTRACT. This paper presents the basic design of the Gemini Near-Infrared Imager (NIRI) and discusses its capabilities. NIRI offers three different pixel scales to match different operating modes of the Gemini telescope and allows polarimetric and spectroscopic observations. It is equipped with an infrared on-instrument wave-front sensor (OIWFS) to allow tip-tilt and focus correction even in highly obscured regions. The science detector array is an Aladdin II InSb 1024 × 1024 pixel device sensitive from 1.0 to 5.5 μm.

1. INTRODUCTION

The Gemini Near-Infrared Imager (NIRI) is the primary near-infrared (NIR) imaging instrument at the Gemini North telescope. It was the first of the NIR Gemini facility instruments to be completed and therefore was intended to also serve several telescope commissioning tasks. NIRI is designed to operate under both diffraction-limited and seeing-limited conditions. It has a common collimator and cold stop, and three cameras of different focal length. The first, named f/6 after the final f-ratio on the detector, has a pixel scale of 0.″117 pixel^{-1} and covers a field of 120″ × 120″ to give Gemini a moderate wide-field capability using tip-tilt compensations and low-order active optics corrections for focus and astigmatism. The second pixel scale, f/14, has a pixel scale of 0.″050 pixel^{-1} and a 51″ × 51″ field. Unlike the f/6 camera, its f-ratio is sufficiently slow that the infrared background fluxes allow imaging in the *L* and *M* bands. The third and finest pixel scale, f/32 with 0.″022 pixel^{-1} and 22″ × 22″ field, is designed to Nyquist-sample the diffraction pattern in the *H* band and will be used with the Gemini adaptive optics system "Altair" (Saddlemyer, Herriot, & Veran 2000).

NIRI is equipped with a pupil-viewing optical system, imaging the instrument pupil onto the science detector array. While not used directly for observations, this system serves multiple engineering functions.

An important feature of NIRI is the infrared on-instrument wave-front sensor (OIWFS) that provides centroid and focus information to the tip-tilt secondary mirror and astigmatism measurements to the primary-mirror support system. For many operating modes of NIRI, a guiding precision of better than 0.1 pixels hr^{-1} is required in order not to significantly degrade the image quality delivered by the telescope. Differential flexure between the guider and the science module must therefore be minimized in order to limit the deterioration of the detected image quality by image motion on the science detector. For the fine pixel scales, in particular, this imposed a requirement for extreme stiffness of the instrument that could best be met by incorporating the guiding functions into the cryostructure of the instrument. Further, with Gemini being an infrared optimized telescope, it is desirable to be able to guide at NIR wavelengths. Infrared guiding provides a larger selection of guide stars in areas of high extinction and allows guiding to continue into twilight when the science infrared detector is still quite capable of obtaining good data.

Over the course of the NIRI project, many individual aspects of its design have been reported in a series of SPIE conference proceedings by Hodapp et al. (1998, 2000, 2003), Young et al. (1998), Bell et al. (1998), Douglass et al. (1998), Thornton et al. (1998), and Hora et al. (1995). This paper summarizes the most important design features and discusses some specific issues that proved to be particularly interesting or posed challenges.

2. INSTRUMENT LAYOUT

The NIRI instrument fills almost the full volume allowed for Gemini instruments. Most of the space is taken up by the steel frame that serves primarily to mount the two large cooled electronics cabinets and to route all the cabling from these cabinets to the core of the instrument, the cryostat (Fig. 1). NIRI is mounted to the Gemini telescope instrument support structure (ISS) by a large, weight-relieved steel plate that supports the steel frame and the cryostat separately. The cryostat needs to be very rigidly mounted to the ISS, while the support steel frame can be allowed to flex more.

[1] Institute for Astronomy, University of Hawaii, 640 North A'ohoku Place, Hilo, HI 96720; hodapp@ifa.hawaii.edu.

[2] Gemini Observatory, 670 North A'ohoku Place, Hilo, HI 96720.

[3] Institute for Astronomy, University of Hawaii, 2680 Woodlawn Drive, Honolulu, HI 96822.

[4] Current address: Harvard-Smithsonian Center for Astronomy, 60 Garden Street, MS 65, Cambridge, MA 02138-1516.

[5] NOAO, Kitt Peak National Observatory P.O. Box 26732, Tucson, AZ 85726-6732.

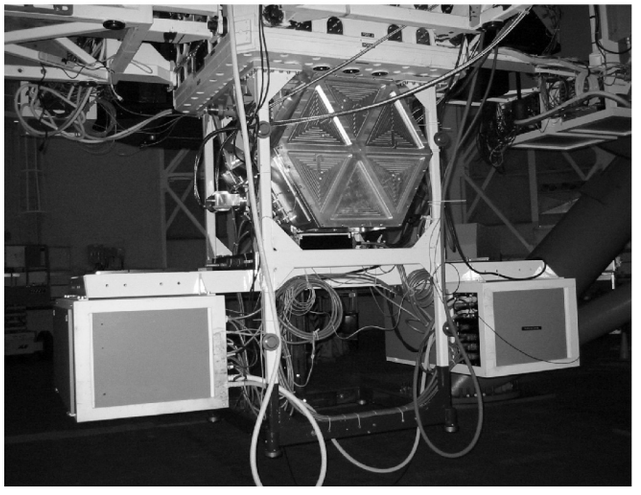

FIG. 1.—NIRI mounted on the uplooking port of the Gemini North telescope ISS. The cryostat is mounted on the ISS through a steel interface plate. The thermally isolated and glycol-cooled enclosures for the support electronics are mounted to the left and right below the cryostat.

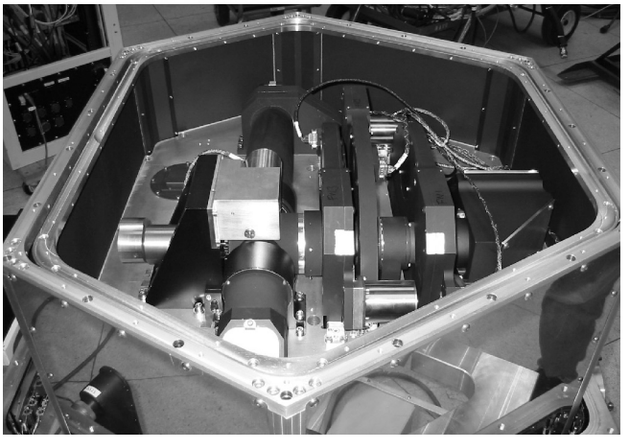

FIG. 2.—NIRI science module. The light goes from the folding mirror at the right to the steering mirror to the left. Visible are the three filter/pupil wheel units with the collimator assembly between two of the wheels.

The NIRI cryostat is of hexagonal shape, so the internal cryogenic components can be mounted on three support points. The internal structure of the NIRI cryostat (Young et al. 1998) is divided into two modules (Hodapp et al. 1998), the science module (Fig. 2) and the OIWFS module (Fig. 3). These two modules are mounted on either side of the central plate that supports the cryostructure. The central plate is connected to the cryocoolers and carries the separate science detector unit. This design allows either module to be removed for maintenance or optical alignment without having to disassemble the thermal connections to the coolers and heaters or the electrical connections to the science detector array.

Each optical module (Young et al. 1998) is essentially designed as a table, with optics mounted on both sides of the table surface. When mounted against the cryostat central plate, the optical modules form an extremely light-tight space below their surface. In the case of the science module, this space provides the proper low photon flux environment for the ALADDIN science detector array, which is sensitive out to 5.5 μm and is therefore very susceptible to even small thermal photon leaks. The fully assembled NIRI cryostructure is extremely stiff, to minimize differential flexure between the science detector and the OIWFS.

3. OPTICAL SYSTEM

As an overview of the NIRI science module optical path, the ray trace of the f/6 camera system is shown in Fig. 4

One important goal in the NIRI optics design was to minimize instrument contributions to the overall system emissivity. The Gemini North telescope was carefully optimized for near-IR and thermal-IR observations to take advantage of Mauna Kea's dry and stable atmosphere. The telescope mirror coatings are aluminum at present, but in the future protected silver coatings will be applied to further decrease the telescope emissivity. At present, with aluminum coatings, the total system emissivity including all NIRI optics is just under 10%, while the silver coatings are expected to give 4% total emissivity.

3.1. Dewar Window

Beside the design of the cold stop and the ability to precisely align this stop, emissivity is controlled by careful design of the Dewar window and the first few components behind the window that could potentially scatter thermal radiation from outside of the telescope optical path into the instrument optical path.

The Dewar window is made of CaF_2, a material of very high transmission (i.e., low emissivity) and low internal scattering. Both window surfaces are broadband antireflection coated to minimize the ghost reflections between them. The large window will cool by radiation into the cold components of the instrument, and its center stabilizes at a temperature below ambient temperature. In order not to impose additional operational constraints on the atmospheric humidity conditions, the window front surface is constantly flushed with ambient-temperature dry and clean air. To minimize the problem of dust particles getting stuck on the front surface of the window, the air flow can be ionized so that dust particles get discharged and do not become electrostatically attracted to the window.

3.2. Beam Splitter

The first optical element behind the Dewar window is the beam splitter that reflects the science field toward the focal plane mask wheel and into the science module. The remaining field of view of NIRI outside of the science field continues on into the OIWFS, so that a suitable guide star can be selected.

NIRI has three beam-splitter mirrors mounted on a large

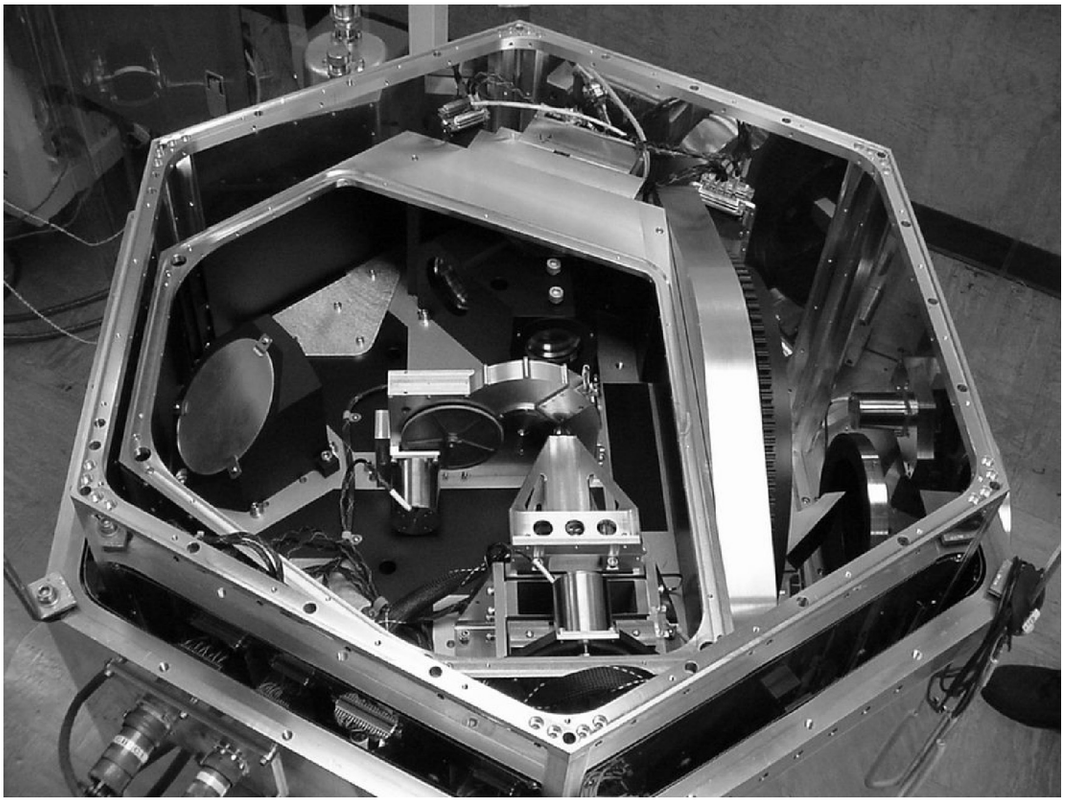

FIG. 3.—OIWFS module of NIRI. Light passing by the science pick-off mirrors on the beam-splitter wheel (*right*) enters the OIWFS below the work surface and is then folded onto the top of the work surface. The collimator is the lens system to the left of the combination lens mount located in the upper part of the image. The gimbal mirror (*top*) selects one guide star out of the field and directs its light through the camera (right side of combination lens mount) and the filter/aperture wheel into the Shack-Hartmann unit on the focusing stage (*bottom*).

turret (Fig. 5), one for each of the three science cameras, so that we can always use the smallest beam-splitter mirror appropriate for a given science camera. The beam-splitter mirror matching the f/6 camera is quite large and leaves only a practically unusable small region for OIWFS guide stars. In practice, guiding for the f/6 camera is provided by the Gemini peripheral wave-front sensors. The beam-splitter mirrors for f/14 and f/32 are smaller and usually allow the selection of a suitable star for OIWFS guiding in the near-infrared.

The optical surface is generated on the electric discharge–machined (EDM) aluminum part by replicating an optical flat onto an epoxy layer on this part and then depositing a gold coating. The process is analogous to the more familiar process of replicating diffraction gratings. Tests of the optical quality of the surfaces produced this way, at both ambient and cryogenic temperatures, demonstrated that the surface quality exceeded our requirement.

3.3. Camera Optics

The rest of the NIRI science optical system is a fairly conservative combination of field lens, collimator, and camera. The design of the optical system is a careful balance of several design goals:

1. to minimize the optical path length,
2. to minimize the pupil size,
3. to provide a long collimated light path for a filter wheel and the pupil wheel, as well as a steering mirror,
4. to be telecentric to minimize plate-scale changes as a result of refocusing.

The ZnSe field lens is located 100 mm behind the focal plane, to avoid reimaging lens imperfections onto the detector. The collimator is a BaF_2 and LiF doublet, forming a 38 mm diameter image of the Gemini telescope pupil in the plane of the pupil wheel, where the cold Lyot stops and dispersive optical elements (grisms and the Wollaston prism) are mounted. NIRI has one filter wheel in front of the collimator, i.e., in the f/16 beam, and another filter wheel in the collimated beam. Filters in the collimated beam are inclined by 5° to prevent "narcissus" ghost images from being refocused onto the detector. The other filter wheel in the converging beam is less susceptible to this type of ghost images and is therefore used for filters that were not designed for a 5° tilt, in particular for

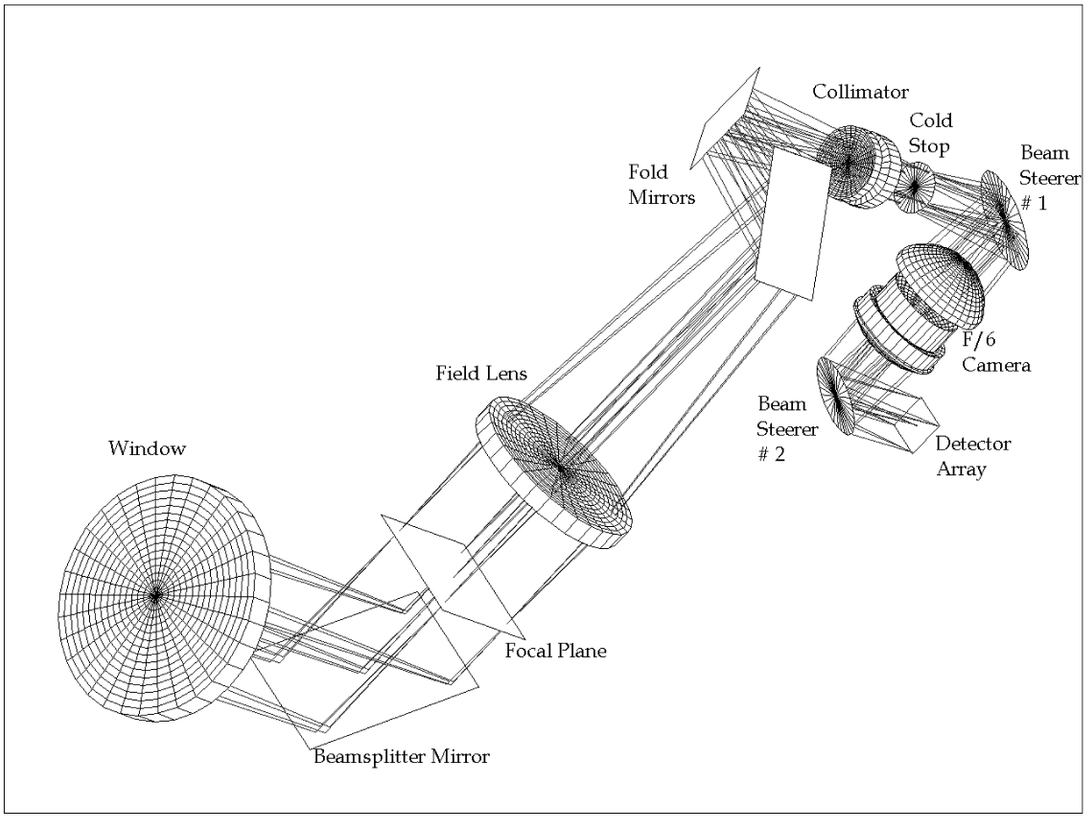

FIG. 4.—Ray trace of the f/6 camera.

the "Mauna Kea standard" broadband filters (Tokunaga, Simons, & Vacca 2002).

NIRI uses three cameras for the three different pixel scales. The cameras use combinations of BaF_2, ZnSe, LiF, and ZnS lenses (always in this sequence) and are designed to be telecentric, so that focus changes are not associated with pixel scale changes. All lens surfaces are spherical, except for one aspheric surface on each of the ZnSe and ZnS elements in the f/6 camera.

The alignment of the individual lenses in their lens cells relies entirely on the mechanical precision of the lens and of the cell. With proper assembly procedures, the relative position of the individual lenses in each group was within specifications.

The optical path of all cameras is enclosed in baffle tubes, with only minimal gaps at the interface to moving elements such as the filter wheels, the steering mirrors, and the focus stage. The baffles distributed inside of these tubes along the optical axis are carefully matched to the size and shape of the optical footprint at their location.

In the design of the camera optics, the focus position was left as an adjustable parameter, so that the requirements for chromatic correction of the optics could be relaxed. Consequently, the science detector is mounted on a focusing stage with ± 3 mm travel to allow the focus to be adjusted for each filter.

The design image quality for the f/14 and f/32 lens systems has all the geometric ray-trace spots in an area smaller than one 27 μm pixel for each filter, assuming refocus between filters. The optical system as fabricated and installed achieves excellent image quality within the expected fabrication and alignment tolerances, and within the science image quality requirements. Using the internal calibration source in the Gemini adaptive optics system Altair, NIRI f/32 images with a Strehl ratio of 87% were obtained at 2.12 μm. Observations of celestial objects in H and K routinely achieve FWHM of 0.″06.

For the wide-field f/6 system, some compromises in the design optical quality were accepted to achieve a very wide field within the constraints imposed by other instrument requirements. While the geometric optical design achieves 80% ensquared energy in one 27 μm pixel in each filter, low-intensity residual coma up to 6 pixels wide was accepted in the field corners. To compensate for fabrication tolerances, the lens spacing in the f/6 camera lens group was adjusted after the first laboratory measurements of the image quality. Thereby, the residual coma of the optical system could be reduced close to the design value and to within the image quality requirements.

3.4. Grisms

The NIRI optical system with its collimated light path was designed to provide grisms for low-resolution spectroscopy

FIG. 5.—NIRI beam-splitter wheel during assembly, seen from the bearing surface (*bottom*). The pinhole mask (*bottom*) is used for instrument alignment and image quality checks. The large pick-off mirror for the f/6 camera is to the left; it effectively blocks all the light from continuing on into the OIWFS. The f/14 pick-off mirror (*top*) and f/32 pick-off mirror (*right*) allow the selection of a guide star very close to the science field.

with the f/32 camera and diffraction-limited slit widths. When used in conjunction with the Gemini adaptive optics system Altair, this NIRI capability of obtaining spectra with extremely fine spatial sampling is unique among the planned Gemini infrared instruments. Due to the long camera focal length and the low dispersion, the grisms for this mode of operation are simple surface-replicated grisms made of infrared-grade fused silica. The grisms were fabricated by Richardson Grating Laboratory by replication from standard master gratings. The *J*-band grism has 9°.6 angle and 75 lines mm^{-1}, the *H*-band grism has 11°.95 angle and 50 lines mm^{-1}, and the *K*-band grism has 13°.35 angle and 75 lines mm^{-1}.

Fairly late in the project it was decided that NIRI should also be equipped with higher dispersion grisms for use with the f/6 camera in seeing-limited observations. These grisms serve to provide low-resolution NIR spectroscopic capabilities from 1 to 5 μm (in the *J* through *M* bands). To obtain the highest possible dispersion within the space constraints of the already existing pupil wheel, these additional grisms were directly ruled into a high refractive index material. We chose KRS5, a mixture of TlI and TlBr that is soft enough to be ruled and available in the required sizes from Zeiss Jena. The grism angle was chosen to be 15°, the maximum allowed by the mechanical constraints of the pupil wheel. The rulings are 317 lines mm^{-1} (*J*), 227 lines mm^{-1} (*H*), 169 lines mm^{-1} (*K*), 105.6 lines mm^{-1} (*L*), and 73.8 lines mm^{-1} (*M*) at the operating temperature of 65 K. All the grisms cover one entire atmospheric band when used with the f/6 wide-field camera of NIRI, and typical slit widths in this configuration range from 0″.23 (2 pixels) to 0″.70 (6 pixels). To provide added coverage at the blue end of certain atmospheric windows, additional offset slits have been installed in NIRI, and special order-sorting filters extending beyond the limits of the photometric broadband filters are used (see Table 1). In practical experience, the KRS5 grisms deliver spectral resolutions slightly below the theoretical expectations. Therefore, they are not being used with narrower slits and with the f/14 camera, since the longer camera leads to less spectral coverage while the spectral resolution is limited by the grism to be no better than what can be adequately sampled by the f/6 camera.

3.5. Wollaston Prism

The NIRI pupil wheel contains a Wollaston prism to allow polarimetric observations. This prism separates the ordinary

TABLE 1
NIRI f/6 Camera Spectroscopic Capabilities

Band	Spectral Range		Resolving Power
	Centered Slits (μm)	Shifted Slits (μm)	(6 pixel–2 pixel)
J	1.03–1.40	0.99–1.35	460–770
H	1.41–1.93	1.35–1.84	520–1650
K	1.90–2.49	...	520–1300
L	2.95–4.11	2.80–3.93	460–1100
M	4.45–5.45	...	460–1100

and extraordinary beams to produce two separate, orthogonally polarized images of any object in the field. The image separation is limited by the thickness of the prism allowed by the pupil wheel and the choice of material. In addition, the separation is also limited by the requirement that the wavelength-dependence of the beam separation will not degrade the image quality in broadband filters. The NIRI Wollaston prism is made of MgF_2, a common choice for Wollaston prisms, and is 13 mm thick with a 10° prism angle. The two components of the Wollaston prism are optically contacted, to minimize reflection losses and ghost images without the risk associated with cementing elements intended for use under cryogenic conditions.

The Wollaston prism separates the two beams by the equivalent of 3.″8 in the Gemini telescope focal plane. It requires a focal plane mask with alternating opaque and transparent stripes, to avoid overlap of the images in the two polarization directions. The resulting image on the detector is two images of each of the transparent stripes, in two orthogonal polarization directions. To cover an object completely, at least two images at different telescope positions (offset by 3.″8) are required. The polarization plane can be modulated by a half-wave plate in the Gemini Facility Polarization Modulator in the instrument support structure (ISS). Due to the location of this modulator, polarimetric observations can be performed only when NIRI is mounted on the up-looking ISS port (as in Fig. 1).

3.6. The Pupil Viewer

NIRI is equipped with an optical system that images the telescope pupil onto the science detector array. This system served an important function in the early commissioning of the instrument at the telescope, allowing a precise optimization and alignment of the Lyot stops with the telescope pupil, thereby minimizing the thermal background reaching the detector. It has already proven useful in identifying warm telescope components protruding into the optical path of the telescope and is being used to characterize the quality of mirror coatings of the telescope. Also, the pupil viewer is now routinely used to verify the position of the Gemini science fold mirror. In the future, the pupil viewer will be used to check the quality and proper alignment of Lyot stops and apodized pupil masks for coronagraphic observations.

The pupil viewer is a system of two lens groups inserted into the f/32 science camera before and after the two folding mirrors. The first group is a combination of ZnSe and BaF_2 lenses, and the second is a single ZnSe lens. The use of a high refractive index material allowed us to achieve the required optical power with relatively thin and lightweight lenses. Since this system had to be chromatically corrected for only two passbands (*K* and *L*), the addition of a single BaF_2 lens to the two ZnSe lenses was sufficient to produce this correction.

3.7. The OIWFS

The Gemini telescope relies on a system of wave-front sensors to actively correct tracking errors, mirror support changes, and telescope flexure. The peripheral wave-front sensors measure tip-tilt, focus, and higher order wave-front aberrations at optical wavelengths on stars usually located 5′–7′ from the field center, well outside the science instrument field. The peripheral wave-front sensor will partially vignette the science field for stars closer than ≈5′ from the center of the NIRI field of view. A view from one of the Gemini Observing Tool (OT) screens illustrates a typical configuration of the peripheral WFS and the OIWFS relative to the science field of view (Fig. 6).

The OIWFS is designed to remove flexure of the instrument relative to the telescope ISS that, of course, cannot be sensed by the facility peripheral wave-front sensors inside the ISS. The NIRI OIWFS has a four-spot Shack-Hartmann wave-front sensor that can provide guiding, tip-tilt, focus, and astigmatism corrections. The focus correction will be particularly important in the future when laser guide stars are implemented with the adaptive optics system. Figure 7 shows an image of the four Shack-Hartmann spots produced by a star.

Early in the conceptual design of NIRI it became clear that the OIWFS should be built into the instrument cryostructure itself, rather than mounted on the outside of the cryostat, to minimize differential flexure between the OIWFS and the NIRI science module. Having decided to locate the OIWFS inside the cryostat and to cool it to the same temperature as the science module, we considered the option of using an infrared detector array for the wave-front sensor. We were encouraged by the test results obtained with the first HAWAII-I detector arrays manufactured by Rockwell under contract from the IfA (Hodapp et al. 1996). These tests indicated that with multisampling, an equivalent read noise between 6 and 7 e^- rms was readily achievable over an 8 × 8 subarray and at frame rates of 100 Hz (Hodapp et al. 1996).

For nighttime wave-front sensor operation at about 100 Hz frame rate, dark current does not significantly contribute to the total noise. For the Gemini telescope and the large pixels (0.″17) used for the OIWFS, the background level obtained under typical conditions in the *H* band will lead to a shot noise only slightly smaller than the multisampled read noise of 6 e^- rms. Further substantial improvements in the read noise over the levels routinely achieved with HAWAII-I infrared arrays are therefore not required for this particular application.

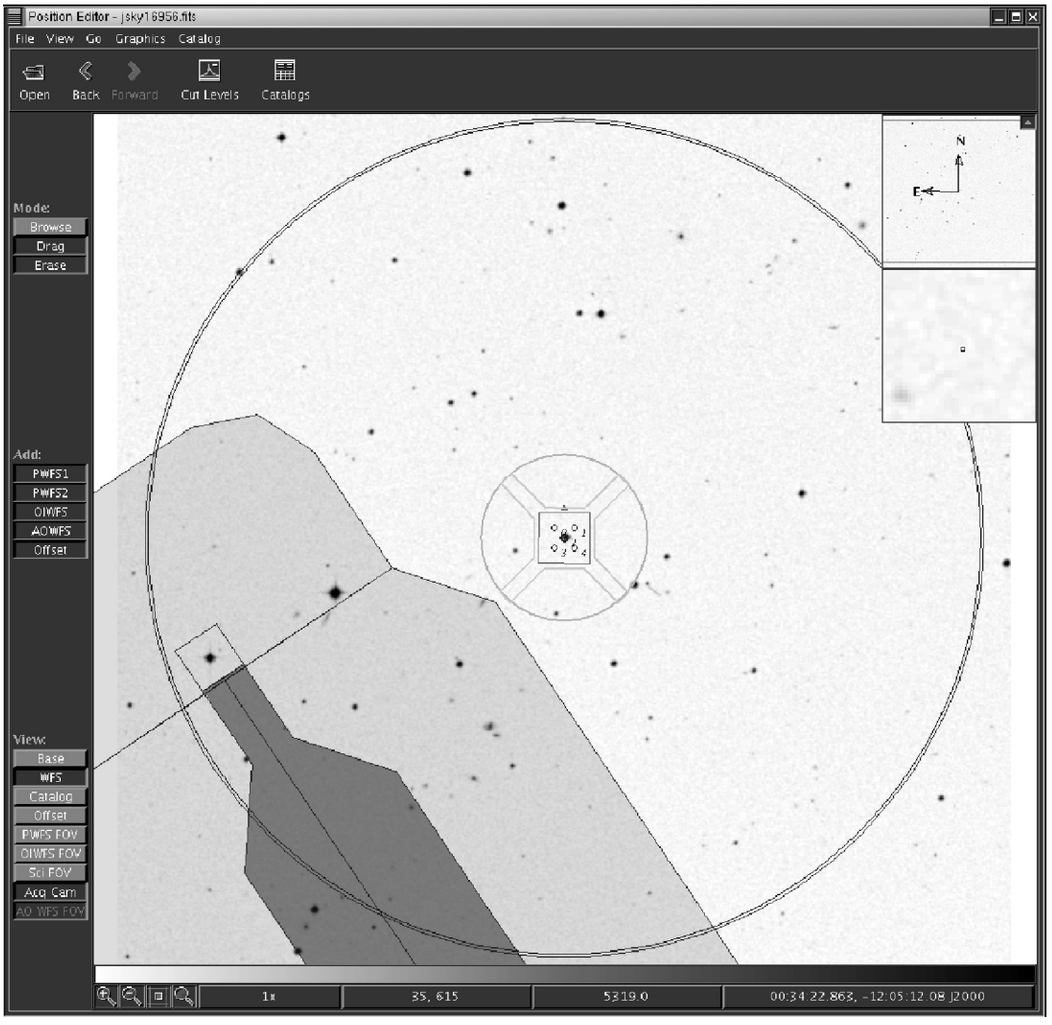

FIG. 6.—OT also has an image display tool. In the example presented here, the NIRI f/14 camera field of view is shown as the small square in the center. The field of view accessible to the OIWFS is the small circle surrounding the f/14 science field of view. The cross-shaped zones are the vignetted areas caused by the support vanes of the f/14 pick-off mirrors (see Fig. 5). The peripheral wave-front sensors are shown as shaded regions, indicating their positions and partial or complete vignetting. Stars within the outer circle are accessible to the peripheral wave-front sensors. OIWFS stars must be found within the inner circle and outside of the inner square and the vignetting of the support vanes.

We have to use a fairly large pixel scale to minimize the number of pixels covered by the Shack-Hartmann spots and to thereby minimize the time required for subarray readout. Detailed modeling of the performance of the NIRI OIWFS resulted in the choice of $0\farcs17$ pixel^{-1} for the pixel scale. Since we are guiding high-resolution science cameras with fine pixels ($0\farcs022$ in the case of the f/32 camera) with much coarser OIWFS pixels, the rigidity against lateral translation in the OIWFS system must be about an order of magnitude higher than in the science cameras if OIWFS flexure is not to dominate the total flexure. Fortunately, the linear range of focus motion required for the OIWFS is much smaller than for the science detector, so that a very stiff flexure stage with only a small range of motion could be designed. In spite of the rigidity of the OIWFS stage, some flexure between the science camera and the OIWFS is still present (most likely due to the gimbal mirror supports). This residual flexure will be characterized and removed using guide-star coordinate offsets calculated by the telescope control system.

Comparing the expected performance of an infrared OIWFS to a similar system operating in the *R* band, the infrared system has a slight performance advantage even under dark sky conditions. The reasons are that the most common stars (K and M types) emit most of their photons in the *J* and *H* bands, more than compensating for the higher noise due to sky background and read noise at these wavelengths. The optimum filter

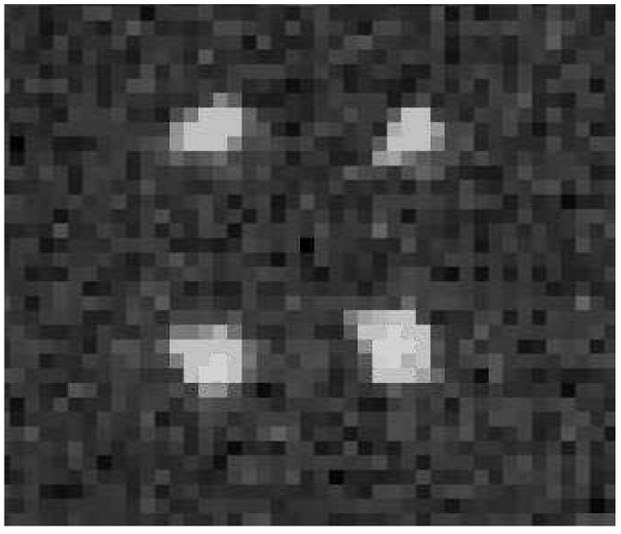

FIG. 7.—NIRI OIWFS Shack-Hartmann spots produced by a star. The separation of the spots is a measure of focus, while the horizontal and vertical separations measure astigmatism.

for use of the NIRI OIWFS outside of dark clouds would be a very broad filter covering the *J* and *H* atmospheric windows. However, such a filter has not yet been purchased for NIRI. An added advantage of infrared wave-front sensing is that the image quality is better in the near-infrared than at optical wavelengths, leading to a better concentration of the available light. The biggest advantage of near-infrared wave-front sensing is the availability of guide stars in dark clouds, enabling the use of Gemini for the study of nearby, heavily obscured star-forming regions. For such deeply embedded guide stars, the *K* filter is usually the best choice.

Even in twilight and after sunrise, an infrared wave-front sensor will continue to operate. In the *K* band, which is most suitable for daytime wave-front sensing, the detector operates in a background-limited regime with shot noise of about 30 e^- rms. This represents a loss of slightly more than 1 mag in guide-star limiting magnitude compared to nighttime observations. For galactic objects, in particular, there is still a high probability of identifying suitably bright guide stars. For observations in the *L* and *M* bands, guiding in the infrared can extend the available observing time by a few hours after sunrise. The limitation to daytime observing will be the deteriorating seeing once the soil on Mauna Kea begins to warm up.

The NIRI OIWFS optics are a refractive design, basically consisting of a field lens, collimator, camera, aperture mask, and Shack-Hartmann optics. Figure 8 shows the optical layout, and Figure 3 shows the mechanical implementation of the OIWFS. The pupil is located in the collimated light path, just beyond the collimator. At this location, a flat mirror on a gimbal stage directs the light of the selected guide star into the OIWFS camera that focuses the image of the selected star onto an aperture mask and filter combination located in the filter wheel. The light of the star is thus spatially isolated from the rest of the field and continues on into the Shack-Hartmann optics and then onto the HAWAII-I detector array, which are jointly mounted on a focus stage.

4. MECHANICAL DESIGN

4.1. Instrument Cooling

NIRI is cooled by two large, two-stage closed-cycle cryocoolers (Leybold Coolpower 130), each with nominal 130 W cooling power in the first stage. NIRI has a large cold mass, and consequently the cooldown takes 6 days even with these big coolers. We have considered an LN_2 precool system to speed up the initial cooldown but have not implemented such a system out of concern over its reliability, safety, and the labor-intensive nature of an LN_2 precool operation.

The base structure of NIRI is cooled down by the first stages of the two coolers and reaches a temperature of 65 K after 6 days. Separate temperature-control loops are used to stabilize the temperature of the science and OIWFS detector arrays and the main mass of the instrument. A temperature of 65 K for the instrument is cold enough that even surfaces directly facing the detector will not emit enough photons to rival the dark current of the ALADDIN detector array. The OIWFS module, being an integral part of the cryostructure, is cooled to the same temperature, even though its emission is far less critical. The OIWFS detector is operated at 80 K, where the HAWAII-I array works best. The ALADDIN detector array is coupled to the second stage of one of the coolers through a long copper strap and a temperature-controlled thermal buffer mass. The ALADDIN array nominally operates at a temperature of 33 K that is easily achieved by the second stage of one of the cryocoolers.

The second stage of the other cryocooler is connected to a cryopump, a combination of charcoal getter and several metal surfaces. At the temperature of 9 K that this cryopump ultimately reaches after 5 days, all constituents of air freeze out at low vapor pressure, so that a high vacuum quality is maintained even in the presence of O-ring diffusion and minor vacuum leaks.

4.2. Radiation and Photon Shielding

NIRI uses several levels of radiation shielding to reduce the thermal load to an acceptable level. The first is a floating shield mounted on the inside of the vacuum vessel walls. This shield, casually referred to as "wallpaper," is made of thin, highly polished stainless steel sheet metal with a gold coating (Eppner Laser Gold). It is mounted with plastic spacers of low thermal conductivity about 3 mm from the inner walls of the vacuum vessel. Being gold coated and highly polished, this "wallpaper" provides a lower surface emissivity than the rough-polished

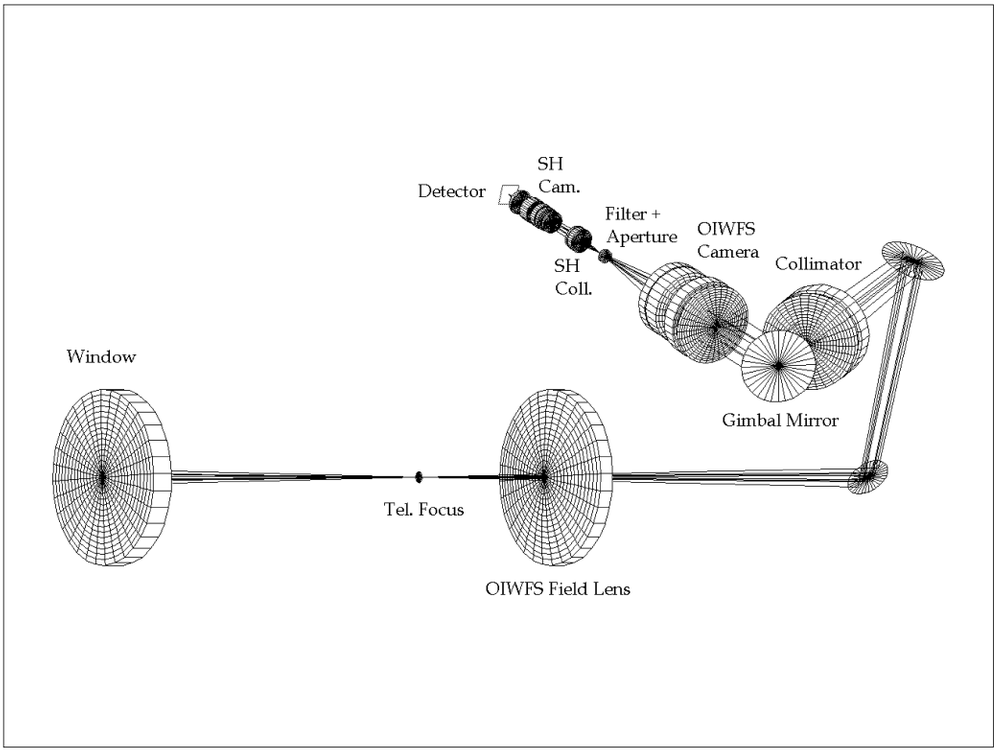

FIG. 8.—NIRI OIWFS optical path. While the OIWFS is typically used with an off-axis star, for clarity we are showing the ray trace of a star on the optical axis.

inner surfaces of the aluminum vacuum vessel. Isolated from the vacuum vessel, it will achieve thermal equilibrium at a slightly lower temperature than the vacuum vessel itself, which leads to a significant reduction in the total heat load onto the cryostructure due to the T^4 power dependence of total emitted power. The cryostructure is covered by cooled, polished aluminum radiation shields that are heat-sunk to the central plate. Inside of these radiation shields, thermal radiation loads are very low, and high surface emissivity is therefore no longer a disadvantage. The inside surfaces of the radiation shields are therefore painted flat black to absorb as many stray photons as possible. In addition, both modules of NIRI are covered by a black painted shield, to further reduce the instrumental thermal photon background. To distinguish these shields from the radiation shields, we refer to them as "photon shields."

4.3. Cryogenic Wheel Support

NIRI contains several wheel mechanisms:

the massive beam-splitter turret,
the large focal plane mask wheel,
two science-filter wheels,
the science-pupil wheel, and
the OIWFS filter and aperture wheel.

For all these wheels, we are using a thrust bearing to support the wheel axially at about half its overall diameter and a central bushing for radial support (Bell et al. 1998).

The thrust bearings are integrated into the wheel itself and its support surface. They consist of a V-groove machined into the support plate, which is hard-anodized and Teflon-coated. The matching surface on the wheel is a flat surface, again hard-anodized. The bearing balls (typically 12) are ceramic balls made of sapphire or tungsten-carbide. They are kept in a ball cage made out of aluminum, but with an insert made out of Teflon or MoS_2-impregnated Vespel that forms the cage for an individual ceramic ball. The choice of materials ensures a long lifetime of the bearing surfaces and an adequate degree of self-lubrication.

The wheels are radially supported by bushings of a variety of designs. We have chosen bushings over bearings early in the project out of concern over the reliability of ball bearings. The bushings have, however, exhibited their own set of reliability problems. Based on the experience with highly preloaded bearings in other NIRI mechanisms, ball bearings would probably have worked just as well for the radial support of the large wheels discussed here. For wheels of relatively loose positioning tolerances, we used a combination of self-lubricating MoS_2-impregnated Vespel and aluminum bronze. With proper tolerancing, these bushings are performing well and are durable. For mechanisms with tighter tolerances, in particular

for the beam-splitter mechanism, we used the combination of aluminum bronze and hardened steel (440C), two materials of very similar thermal expansion coefficients. In addition, the interface is dry-lubricated with MoS_2 powder.

4.4. Geneva Mechanism for Wheels

All the optical component wheels in NIRI are designed with the same type of Geneva mechanism. The basic design of this mechanism and some early test results were described by Bell et al. (1998). The Geneva mechanism translates the constant velocity of the cam with its two drive pins into a varying velocity motion of the wheel with a dwell position where the drive pins decouple from the wheel. This mechanism is therefore well suited for wheels that position optical elements in a number of discrete positions. In the dwell position, the wheel is decoupled from the drive pins, i.e., from the motor and its gears, allowing the position of the wheel to be determined by a detent mechanism without any interference by the drive mechanism.

The detent mechanism is a spring-loaded detent arm that pushes a ball or pin into a groove on the wheel and thereby determines the precise position of the wheel. The detent arm is actuated by a cam mechanism that is an integral part of the drive pin unit. The cam lifts the detent ball out of the groove before the wheel gets out of the dwell and begins to move. When the next dwell position is reached, the detent arm moves inward again until the detent ball engages into the groove. At this point, the detent arm disengages from the cam, making the dwell position independent of the motor position. This process is repeated until the desired position of the wheel is reached. The stepper motor is then turned off to minimize power dissipation in the instrument.

The position decoding for NIRI filter wheels and other rotating mechanisms with discrete position relies on sensing the field of magnets installed on the wheel. The goal was to provide a contact-free method of finding a zero point of the filter wheel motion and to uniquely identify each position, independent from incremental counting of steps.

4.5. The Beam-Steering Mechanisms

NIRI uses two beam-steering mechanisms that, in combination, direct the collimated light into one of the three cameras and from the cameras onto the science detector array. The first of these two beam-steering mirrors is located in the parallel beam created by the collimator and close to the pupil of the optical system. Therefore, in order to preserve the diffraction-limited quality of the images over long integration times, the surface of the mirror has to be stable within a small fraction of the wavelength. For a Cassegrain instrument that has to deliver this level of stability in arbitrary orientation and while tracking the object, this translates into very demanding specifications for support and positioning of this beam-steering mechanism.

The first design that we had developed for this mechanism did not come close to meeting the stability requirements in certain orientations of the mechanism. This original design consisted of a thrust ball bearing supporting the steering mirror in axial direction and a V-grove support in radial direction. The detent arm of the Geneva mechanism also served to press the shaft of the steering mirror into the V-groove, supporting the steering mirror at its center of gravity. In practice, however, we could not make the detent spring strong enough to ensure the proper functioning of this mechanism in all orientations, especially those where the detent spring had to lift the mechanism into the V-groove against gravity. The positioning of the device thus depended, as it turned out, on a precarious balance of spring forces, gravity, and friction. Further, because of its inherent instability, this old design was also susceptible to vibrations induced by the cryocoolers, most notably in the longest focal length f/32 camera.

This original design was abandoned after several attempts to improve its performance and was replaced by a more conventional design consisting of four angular contact ball bearings in a duplex configuration (Fig. 9). This design is similar to bearing designs used for the UKIRT/Gemini instrument Michelle (Glasse, Atad-Ettedgui, & Harris 1997).

The preload on the bearings was controlled with the use of stacked spring washers. The bearings used for this slow-moving mechanism are standard angular contact ball bearings, not specifically fabricated for use in cryovacuum conditions. They were prepared for use in NIRI by careful degreasing, cleaning, and lubrication with MoS_2 powder.

It is critical for the operation of ball bearings that the thermal stresses between the base material of the instrument, typically aluminum, and the steel bearings, are properly managed. For the steering-mirror mechanisms, the bearing housing is made of steel and is sufficiently strong that it is not being significantly compressed by the surrounding aluminum during cooldown. While most of the rotating parts of the steering mirror are made of aluminum, the shaft was made of a steel alloy closely matching the bearing material and was toleranced to a tight sliding fit for installation. The optical component is surface replicated onto a machined-aluminum 6061 T6 block, and the interface to the steel shaft is carefully designed to minimize thermal stresses in the aluminum block and thereby distortions of the optical surface.

4.6. The OIWFS Gimbal Mirror

The OIWFS uses a flat two-axis steerable (gimbal) mirror to direct the light of a selected star within the field of view of NIRI into the Shack-Hartmann optics. This gimbal mirror must be moved over several degrees with high precision and must be stable under changing instrument orientation to meet the image-quality requirements. Under control of the Observatory Control System (OCS; § 8.), the gimbal mirror must be able to move during science observations, so that moving objects

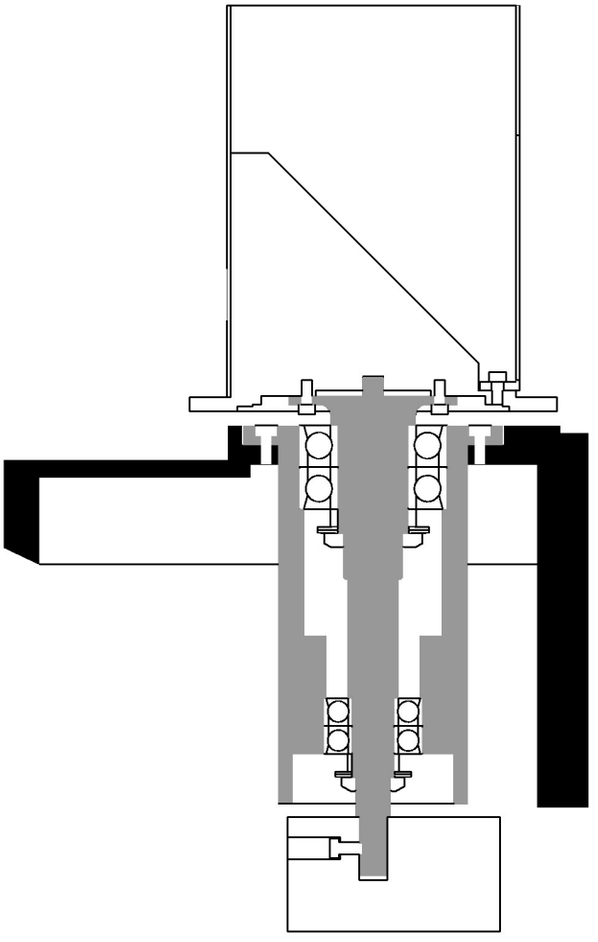

FIG. 9.—Cross section of beam steerer bearing assembly. The steel shaft and bearing housing are shown in gray, while the mechanism mount is shown in black.

can be observed using stationary guide stars. Also, atmospheric refraction corrections between the bandpass used for guiding and the science bandpass require motion of the gimbal mirror during the science integration time. This requirement implies that the motors will be continuously powered so the microstep resolution of the motor, maintained by a balance of the currents through the coils, is preserved. The basic design of the gimbal mount was described by Thornton et al. (1998). While the design was basically kept as described there, several steps were taken to improve its performance.

We use an M8 × 0.7 mm lead screw ground out of hardened steel (440C) and a nut made out of aluminum bronze. MoS_2 powder was distributed in the threads to provide some dry lubrication. The advantage of this material combination is that the steel and bronze have similar coefficients of thermal expansion, allowing to keep a close fit of screw and nut and maintain operability in the cold.

The original design (Thornton et al. 1998) of the gear driving the lead screw contained both a spring antibacklash device and a mechanical stopwork to limit the range of motion. Both these rather complicated mechanical devices failed to perform reliably and were ultimately removed from the design. For backlash correction, we rely entirely on software motor control. To limit the linear motion, additional limit switches were installed that signal a fault condition to the motor controller when the physical limits of travel are about to be exceeded. We have experienced two incidents where this protection proved inadequate, both triggered by electrical hardware problems in the limit switch circuitry that ultimately lead to mechanical damage to the gimbal mechanism. We have not added further safety features but rather rely on better test procedures and problem awareness by the operators to prevent a repeat of these incidents.

4.7. Lens Mounts

The mounting of lenses in a cryogenic environment poses difficult challenges. In the f/6 optical system, the tolerances for relative spacing of the lenses along the axis and for centering perpendicular to the axis are typically on the order of 20 μm, while tilts have to be within arcminutes. Such tolerances are within fabrication tolerances, but the unique challenge of cryogenic lens design is to maintain these tight tolerances at the operating temperature of the infrared instrument and to ensure that the lenses survive the cooldown. The thermal expansion coefficients and integral shrinkage of typical optical materials used in infrared optical systems range from near zero for fused silica to more than the expansion of aluminum for LiF. Even if the thermal expansion properties can be matched, the problem remains that the lens will cool down more slowly than the lens mount and therefore lag behind in shrinkage.

For NIRI, we have chosen a lens cell design derived from the design used in several previous instruments built for the NASA Infrared Telescope Facility (Toomey, Stahlberger, & Watanabe 1994). Lenses are radially supported by two small segments of the proper bore diameter for mounting the lens under cold conditions. A spring is used opposite these two hard points to press the lens against them. This allows the lens to adjust to any mismatch between its shrinkage and the mount without excessive force. In particular, the lens will not be precisely centered at room temperature, but will assume its proper centering once thermal equilibrium at its operating temperature has been established. Axially, the lens is spring-loaded against a reference surface, defining its position along the axis and its tilt. This design relies on the ability of the lens to move during cooldown, and friction effects have to be considered. The two radial hard points are not positioned 120° apart, which might appear as the most natural positioning, but rather at 90°, to reduce the risk of the lens getting pinched between the hard points, since friction between the ground sides of the lens and the cell is high.

For multilens systems, we used spacers between the lenses to establish their axial separation. These spacers have conical surfaces tangential to the spherical surface of the lens in the area supported by the spacer. Finally, the axial preload is applied either by simple wave washers between the end plate and the last lens spacer or by individually adjustable spring-loaded plunger screws.

In our experience, this design of lens mounts worked well for single lenses and for doublet lens systems spaced relative to each other. We have encountered difficulties in assembling the NIRI f/6 camera lenses that have the tightest tolerances of all the lenses in NIRI and use a lens cell with three lenses stacked on top of each other. This lens cell could be assembled only using a precise assembly procedure to ensure that the installation of the next lens would not disturb the alignment of the previously installed lenses. In retrospect, it would have been better to design such tightly toleranced lens systems with sufficient spacing between the lenses to allow them to be individually seated in the lens cell.

4.8. Focus Stages

The two focusing stages for the science detector and the OIWFS are of the same basic design, even though the details differ as a result of different stiffness requirements. The OIWFS focusing stage has the more stringent stiffness requirements, since we are guiding the finer scale science pixels with much coarser pixels on the OIWFS. Therefore, the OIWFS is much less tolerant of lateral displacement of the detector, as discussed in § 3.7. The linear motion is established by a combination of stainless steel lead screw and an MoS_2-impregnated Vespel SP-3 nut. For the slow and infrequent motion of the focusing stage, this material combination, lubricated with MoS_2 powder, proved adequate. The large difference in coefficient of thermal expansion between the steel and the Vespel poses a problem for the matching threads of the screw and the nut. We overcame this problem by iterative cold testing of the interface during the cutting of the threads.

The OIWFS flexure translation stage is fabricated from a single block of Titanium 6Al-4V-ELI material by EDM. The stage is an eight-beam compound flexure with all flexing elements being of the same dimensions, thereby assuring linear motion and a high degree of rigidity against transverse motion (Douglass et al. 1998). The detector module, and the Shack-Hartmann optics in the case of the OIWFS, are mounted on the front surface of the main beam. A counterweight is mounted on the back surface of the main beam to balance the flex stage at its center.

The screw-nut combination used to drive the focus stage mechanism is preloaded by the flexure stage itself, except in the force-free middle position. A small amount of backlash (about 8 μm) is present in the system and is compensated in software by always moving into a given position from the same direction.

5. CONTROL ELECTRONICS

The NIRI control electronics consists of five major components and performs the following functions: (1) operation of the mechanisms in the instrument, (2) control of the cryocoolers, (3) control of cryostat central plate and detector temperatures during both normal and accelerated warmup operations, and (4) operation of both the science and OIWFS detector arrays.

The science detector controller electronics system was not built as part of the NIRI contract but was developed and built at NOAO and supplied to the NIRI project by Gemini.

5.1. Optical Component Controller (OCC)

The Optical Component Controller (OCC) operates NIRI's 14 stepper motors. TTL pulses are generated by two Oregon Micro Systems 8-Channel Intelligent Motor Controllers (VME8-8). These pulses are then fed to a set of Phytron Stepper Motor Drive Modules. These drive modules generate the necessary constant current, two-phase, stepper motor coil-excitation signals required to move the Phytron VSS52 cryotemperature stepper motors. The drive modules keep the total current per pulse at a constant level even when the motor coils change resistance between room temperature and cryotemperature.

The OCC motor drivers are all powered by a common 48 V, high-current power supply. This power supply serves a dual purpose. During accelerated warmup mode, the cryomechanism motors are not in use and supplying power to these motors is not necessary. For fast warmup, the 48 V power is redirected by a manually operated switch to a series of heater resistors located around the perimeter of NIRI's central plate and supplies up to 460 watts of additional power to expedite warmup. This system also assures that the NIRI mechanisms cannot be operated under conditions of fast warmup, where attempts to operate the mechanisms may actually damage them.

5.2. Cryocooler Control Electronics

The cryocooler control electronics was designed to operate the two Leybold Coolpower Model 130 cryocoolers, which are also stepper motor operated.

In computer mode, the cryocooler motor driver receives its TTL pulses from two the motor controller. These pulses are first passed though some circuitry that acts as a "watchdog." Should the pulses cease, or drop below an acceptable (board-settable) rate, they are replaced by pulses generated on the board. Should the computer-generated pulses return, control is returned to the computer. Manual mode simply provides locally generated TTL step pulses for off-line use with a settable speed and ramp-up/ramp-down. The cryocoolers are also protected by pressure fault switches that shut them off in the event of a drop in helium supply pressure.

5.3. OIWFS Detector Control

For the OIWFS, we are operating only one quadrant of the HAWAII-I array. The readout directions of the four quadrants are arranged such that there is only one quadrant (quadrant 3) where the readout starts near the physical center of the full device. Since the edges of hybrid infrared devices typically have a larger number of disconnected bad pixels, quadrant 3 has the lowest density of bad pixels at the beginning of the shift registers, i.e., in the area that can be addressed fastest.

The HAWAII-I detector array is operated by a San Diego State University (SDSU) array controller (SDSU-2). This controller is connected, via fiber-optic cables, to a VME-type interface board located in the Gemini Telescopes component controller VME crate. The interface board was also purchased from SDSU.

The controller consists of one 24 output clock board, one dual-channel IR video processor board, and one generation II timing board. Because only one quadrant of the HAWAII-I detector is needed for NIRI OIWFS operation, only one video processor board channel was connected to the detector. However, both channels were configured identically, with one serving as an emergency backup for the other.

The video processor board also serves as a stable and low-noise source for some of the HAWAII-I detector array's DC voltages. The "biasgate" voltage that sets the output amplifier current and is therefore particularly sensitive to noise is generated on the video processor board, as well as $V_{\rm reset}$, the voltage applied to the integrating node during reset; $V_{\rm source}$, the source voltage for the detector's output FET 10 kΩ load resistor; and $V_{\rm high}$, the analog power for detector's analog circuitry. The remaining, less sensitive voltages were generated on the controller's clock board along with the array's digital clocks.

While the design and performance of the SDSU-2 controller are generally adequate for OIWFS operations, we made improvements to its noise performance. The controller's internal cooling fan generates a fair amount of electrical noise, picked up by the video processor board's preamplifier. The magnitude of the noise is equivalent to a few tens of electrons of equivalent detector signal when channel 1 was used to process the detector signal. Experimentation showed that the cause of the noise was the motor's internal driver circuit, which was used to operate a brush less motor from a DC power source.

Adequate shielding of the motor without severely reducing airflow would have required a major change in the physical design of the box. Fortunately, however, the channel 2 preamplifier is physically located on the opposite side of the video processor board, adding several inches of separation between it and the fan. This distance proved to be sufficient so that the pick-up noise in channel 2 is less than 10 e^- rms, acceptable for the OIWFS.

6. SCIENCE DETECTOR

6.1. The ALADDIN Array

The ALADDIN 1024 × 1024 pixel format InSb SCA (sensor composite assembly) was designed, developed, and funded through the collaborative efforts of the National Optical Astronomy Observatory (NOAO), the United States Naval Observatory (USNO) (Flagstaff), and the Santa Barbara Research Center (now Raytheon Vision Systems) on behalf of the astronomical community. Announced in 1993, the ALADDIN readout integrated circuit (ROIC) has undergone two generations of refinement since the ALADDIN-I prototype: the production-quality ALADDIN-II was redesigned for higher yield, lower read noise, and faster operation; the ALADDIN-III (occasioned by the manufacturing decision to move to larger wafers) was further refined to improve yield and finally meet the original video settling time requirement for 20 Hz frame rate operation. The ALADDIN architecture is described in detail by Fowler et al. (1994, 1996). The Gemini Project procured a set of these production ALADDIN SCAs (a lot run, which yielded 10 devices, nine scientifically useful) for use in instruments such as NIRI and the Gemini Near-Infrared Spectrograph (GNIRS).

Although both the detector material and the readout are seamless, the ALADDIN ROIC is fabricated with four electrically independent quadrants, each with eight independent parallel video outputs. Individual pixels are addressed through row and column shift registers that connect each pixel to its associated output. In detail, rows are selected and then read out eight adjacent columns at a time. ALADDIN SCAs were specifically designed to read the four quadrants in from the corners toward the center to reduce glow within the array, to provide smoothly varying characteristics and time coherency at the quadrant interfaces, and to support fast subarray readout.

6.2. The GNAAC Controller

The ALADDIN array controller, GNAAC, produced to specification for Gemini by NOAO, follows the Gemini design philosophy of placing a complete data acquisition system on the instrument that outputs descrambled and co-added images to the observatory data handling system (DHS) via Ethernet. This arrangement facilitates system operations both on and off the telescope, albeit at the expense of greater complexity close to the instrument.

To operate at high background flux levels, an IR array must be run fast enough to keep the potential wells from saturating. Frame rates approaching 20 Hz are desirable for operation in the *L* and *M* atmospheric windows. To meet this requirement, we have deployed a separate video channel (preamplifier and analog-to-digital converter [ADC]) for each of the 32 independent parallel video outputs with a relatively high bandwidth analog filter (5τ time constant of 1 μs). The fast (2 MHz) 16 bit precision ADCs (Analogic ADC 4322A) required to support

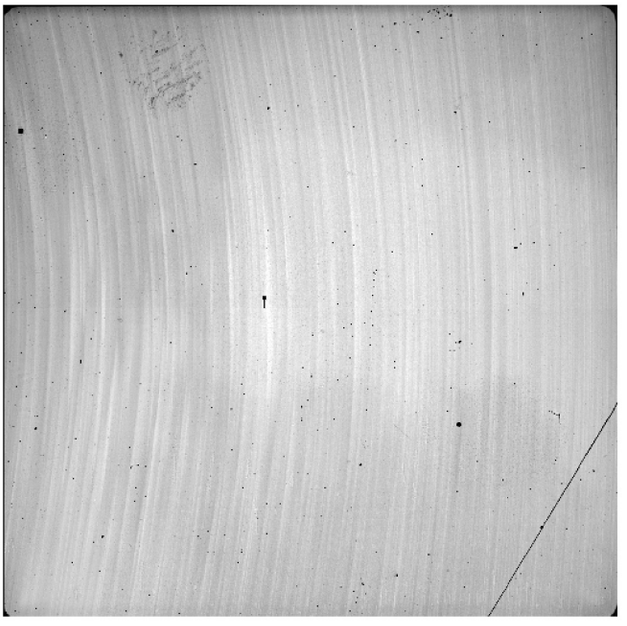

FIG. 10.—*J*-band flat field of the ALADDIN detector array used in NIRI.

operation at these rates are available. We exploit this capability with GNAAC to implement a simple yet powerful digital filter to flexibly reduce the signal bandwidth and reject noise. We have found that by pausing briefly (currently 4 μs) after connecting to a given pixel and then digitally sampling the video signal multiple times (1, 2, 4, 8, or 16 samples), system noise is significantly reduced in about half the time required by more traditional multiple-pole analog filters. The resultant stream of 16 bit digital data is accumulated, normalized to a single sample on the ADC boards, and passed to the data system as a filtered sample.

Modern IR arrays can be read out nondestructively. This means that reading out the array (sensing the charge on each pixel node) and resetting the array (in effect, recharging the capacitance at each pixel node) are distinct operations. Several techniques for resetting the pixels (built into the array readout architecture) have been developed:

Pixel reset.—Each pixel is independently addressed and individually reset.

Row reset.—Each row of pixels within a quadrant is independently addressed and reset at the same time.

Global reset.—All the pixels within a quadrant are reset at the same time.

Earlier InSb arrays have employed the pixel-reset method. Implementation of the pixel-reset mode on a 1024 × 1024 pixel array presents a difficult design challenge involving a million transistors and their associated traces that would be difficult to build with acceptable yield. Instead, the ALADDIN array has been designed to implement the electronically simpler and more practical global-reset and row-reset methods.

For best results, it is necessary to allow a settling time (typically on the order of 2–10 ms) between resetting a pixel and reading it out. The global-reset method has negligible reset overhead, exchanging speed of operation for varying address-dependent time delay between reset and read. At low to moderate background, this time skew is unimportant, and the fast readout time allows room for a high degree of digital signal filtering. At high background, where signal filtering is less important, the row-reset method reduces the time skew at the expense of somewhat slower operation.

It is important to remember that for each pixel the integrating node, which was recharged upon reset, begins to discharge immediately as additional photons are detected. Consequently, there will be a nonzero signal component in the first read whose magnitude is a function of the elapsed time between pixel reset and pixel read. In particular, when the global-reset or row-reset methods are used, this signal will be an increasing function of pixel address. The row-reset method reduces the magnitude of this effect by a factor of 512. The array microcodes currently deployed with GNAAC implement only global reset. Row-reset microcodes are under active development.

6.3. The ALADDIN Array in NIRI

The science array in NIRI is a 1024 × 1024 pixel InSb ALADDIN-II array. In regular science operations, three readout modes are used. For very high background thermal applications, the background can saturate the detector in short exposures, so no digital averaging and only one double-correlated read pair (one Fowler pair) are used to minimize the readout time. The measured read noise in the thermal-IR mode is approximately 100 e^-. If further reductions in readout time are desired, a smaller subarray can be read. For moderate-background wide-field imaging at 1–2.5 μm, 16 digital averages are used to reduce the read noise to approximately 45 e^- rms with only a modest increase in readout time. Only one Fowler pair is used because the background noise is usually much larger than the read noise. For low-background applications, including spectroscopy and narrowband imaging, 16 digital averages and 16 Fowler read pairs are used to achieve the minimum read noise of $\approx$13 e^- rms.

The array chosen for installation in NIRI has good cosmetics (Fig. 10), low read noise, and low dark current. The array has one diagonal crack in the lower right-hand corner and three small patches of dead pixels where "photon-emitting defects" were removed. The number of bad pixels (hot, dead, and inconsistent pixels) is approximately 0.1% of all pixels. The dark current measured in the lab was 0.25 e^- s^{-1}; on the telescope, the dark instrumental background is approximately 0.3–0.5 e^- s^{-1}. For most applications the sky background is much higher than the dark current. A *J*-band (1.1 μm) flat-field image is

shown in Figure 10, in which most of the detector features are visible. The pattern of narrow arcs from milling during array production is completely removed when data are flattened.

Detector read noise and dark current performance as a function of temperature was explored in the laboratory. At temperatures below 30 K, read noise increased significantly. The dark current increased dramatically at temperatures above 35 K. We found the best operating temperature for the NIRI ALADDIN array to be 33 K. The array temperature is kept stable by actively controlling the temperature of both the array mount and a buffer mass that is connected to the second stage of one of the cryocoolers.

The array is normally operated at a bias voltage of 0.6 V that gives a full-well depth of approximately 200,000 e^-. For very high background thermal imaging, the bias voltage can be increased to provide more dynamic range. At 0.9 V, the well depth increases to 280,000 e^- while the number of hot pixels increases to approximately 0.4%. Because the array output is unstable for a few minutes after a bias voltage change, frequent changes in well depth are discouraged. The array is linear to better than 1% for flux levels less than 70% of the full-well depth.

The ALADDIN array is read both before and after the exposure, and the final image is the difference between the two reads. Some flux is accumulated before and during the first set of reads, so the saturation level in the output image is a function of the flux level. An object or background that contributes a significant fraction of the full-well depth before the first reads are complete will show signs of saturation at a lower raw count level than the nominal expected saturation level. Increasing the number of read pairs (Fowler samples) to reduce read noise increases the time between the initial array reset and completion of the first set of reads, thus effectively reducing the available well depth for bright sources. Because the array is read starting from the corners and working inward to the center, the effective well depth is also a function of location on the array. Progressively brighter sources in short exposures will approach saturation and then apparently begin to get fainter as the array approaches saturation in the time between the initial reset and completion of the first set of reads. Saturated stars in short exposures typically appear as bright rings with dark central holes. These effects will be greatly reduced once row-reset capability is implemented. To minimize confusion due to an effectively variable saturation level and to increase observing efficiency, minimum exposure times a few times longer than the shortest possible integration times are recommended. The minimum recommended exposures are 44 s in the low-background mode, 2.7 s for wide-field imaging, and 0.9 s for thermal IR observations (for full array readout).

The ALADDIN array in NIRI shows some image persistence after being exposed to bright sources. A highly saturated star will leave a ghost image at the level of about 1% in the subsequent exposure and 0.2% in the next one. Because residual images make constructing sky frames difficult, it is worthwhile to avoid saturating if at all possible. In most near-IR bands, the background is high enough to allow shorter exposures without becoming read noise limited. Shorter exposures can be coadded internally in the NIRI array controller to produce a final image with the same total exposure time without significantly increasing overheads.

One interesting feature of the ALADDIN array in NIRI is that the background dark current is somewhat dependent on the way the array was read out prior to starting a new sequence of exposures. Typically, the first exposure of a set after a change in array readout configuration or background level (i.e., changing filter or exposure time) is affected by very poor dark subtraction. The pattern of dark current has a large-scale structure that usually renders the first frame unusable. We are investigating this issue, which is most likely related to the image persistence phenomenon. Meanwhile, observers usually take a dummy frame at the start of a sequence to clear the dark-current pattern.

One of the most difficult and persistent problems degrading system performance has been intermittent pattern noise resulting from 60 Hz interference. The 60 Hz noise manifests itself as a diagonal herringbone pattern. Because of the symmetry of the array readout from corner to center, the pattern is reflected in each quadrant. The pickup noise is intermittent, and work is underway to identify and remove it permanently. It is not present in the laboratory and has been eliminated at times on the telescope, indicating that it arises from the telescope environment and not from the NIRI electronics. The telescope environment is constantly evolving, and continued attention to all the details of this environment is required to maintain a low level of pickup noise.

7. SOFTWARE DESIGN

The NIRI software provides control of all mechanisms, feedback on mechanism positions, detector readout and control, and the external interfaces to Gemini facility software and systems. The GNAAC detector controller and interface software runs on one set of Motorola VME-based processors running VxWorks in one of the two thermal enclosures. The control of all NIRI mechanisms (OCC) and the OIWFS detector controller run on similar VxWorks computer systems in the second cabinet (see Fig. 1). The hardware interface was provided via a mixture of commercial and custom VME interface boards.

The Gemini software was developed using the Experimental Physics and Industrial Control System (EPICS), a system for building and testing software for controlling mechanical and electronic components. EPICS includes a software toolkit based around reusable software components (called "records"), a communications protocol, and various development tools.

In addition to the standard EPICS tools, Gemini also provided a software package, known as the Core Instrument Control System (CICS). The CICS was intended to be both a prototype instrument controller and a set of reusable components

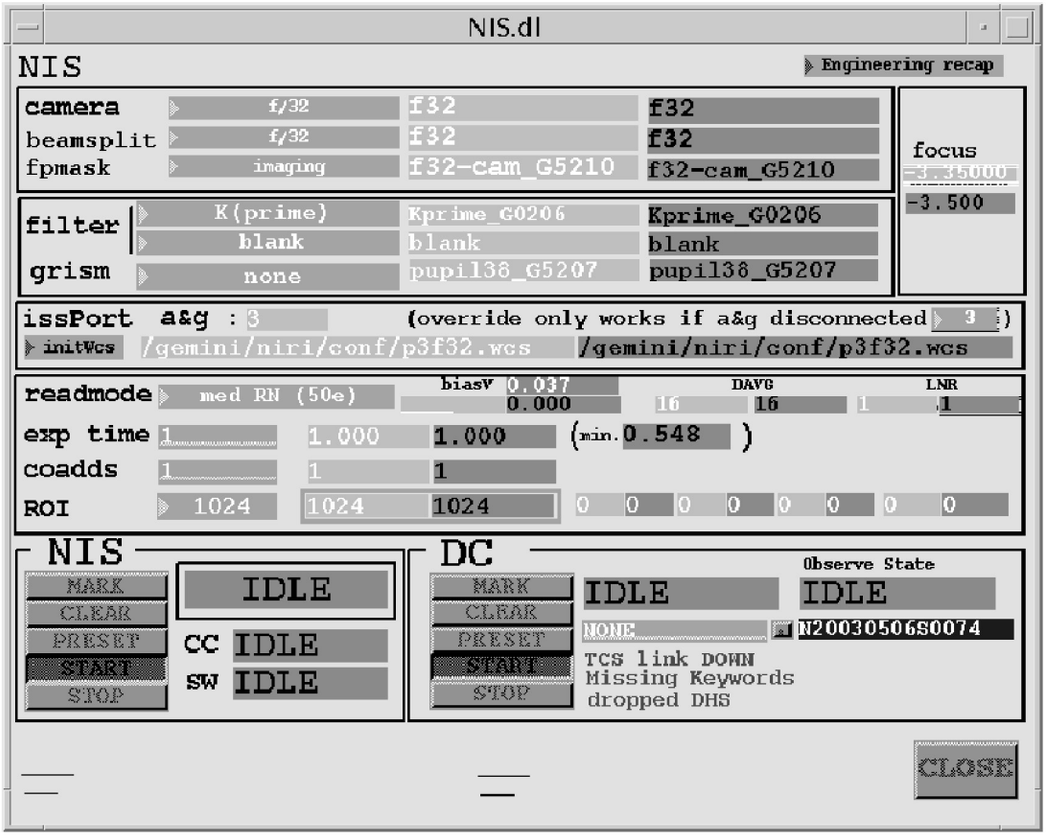

FIG. 11.—Typical engineering interface EPICS screen.

for instrument-software development. It was found that the CICS was a useful starting point, but that it assumed a very simple model for mechanism and motor control. The CICS was unable to make use of the positioning information that was provided by the NIRI Hall-effect sensors and was unable to handle a programmed sequence of operations. The homing algorithms required the mechanisms to be repositioned while collecting data from the Hall-effect sensors. The CICS was rewritten to be able to handle the information from the sensors. A custom motor-control record was written that permitted programmed, coordinated motor movement using the Hall-effect sensors for feedback. The custom motor-control record also used the sensors to detect positioning errors, which was quite useful for detecting and diagnosing hardware problems.

8. OBSERVING WITH NIRI

A number of EPICS screens form the engineering-level interface to the NIRI components and detector (Fig. 11). These screens allow direct access to stepper motor controls, Hall-effect sensor feedback, cryocooler settings, detector voltages, and so forth. They also provide a way to quickly configure the instrument and take engineering data. However, the EPICS screens are not appropriate for conducting science observations or engineering tasks that require sequencing of the telescope or the calibration unit with NIRI, because all operations are manual and therefore inefficient.

Commissioning and science observations are conducted from the high-level control software that interacts with NIRI and many other telescope subsystems. The most recent version of the Observatory Control System (OCS) interfaces the telescope and instrument to the Observing Tool (OT). The OT is the graphical tool used by the astronomer to prepare detailed instructions on how to execute an observation (called the "phase II" proposal). After a particular program has been awarded observing time, the astronomer downloads the latest version of the OT, installs it, and prepares the phase II observing program. The OT is written in JAVA and works on a variety of computer platforms. The phase II program is then sent to Gemini, where staff members check the observations for technical feasibility and load them into the active observing database. Examples of OT screens for the NIRI component of an observation are shown in Figures 6 and 12.

The OT is also used to execute the observations at the telescope. Within the phase II program are elements that configure

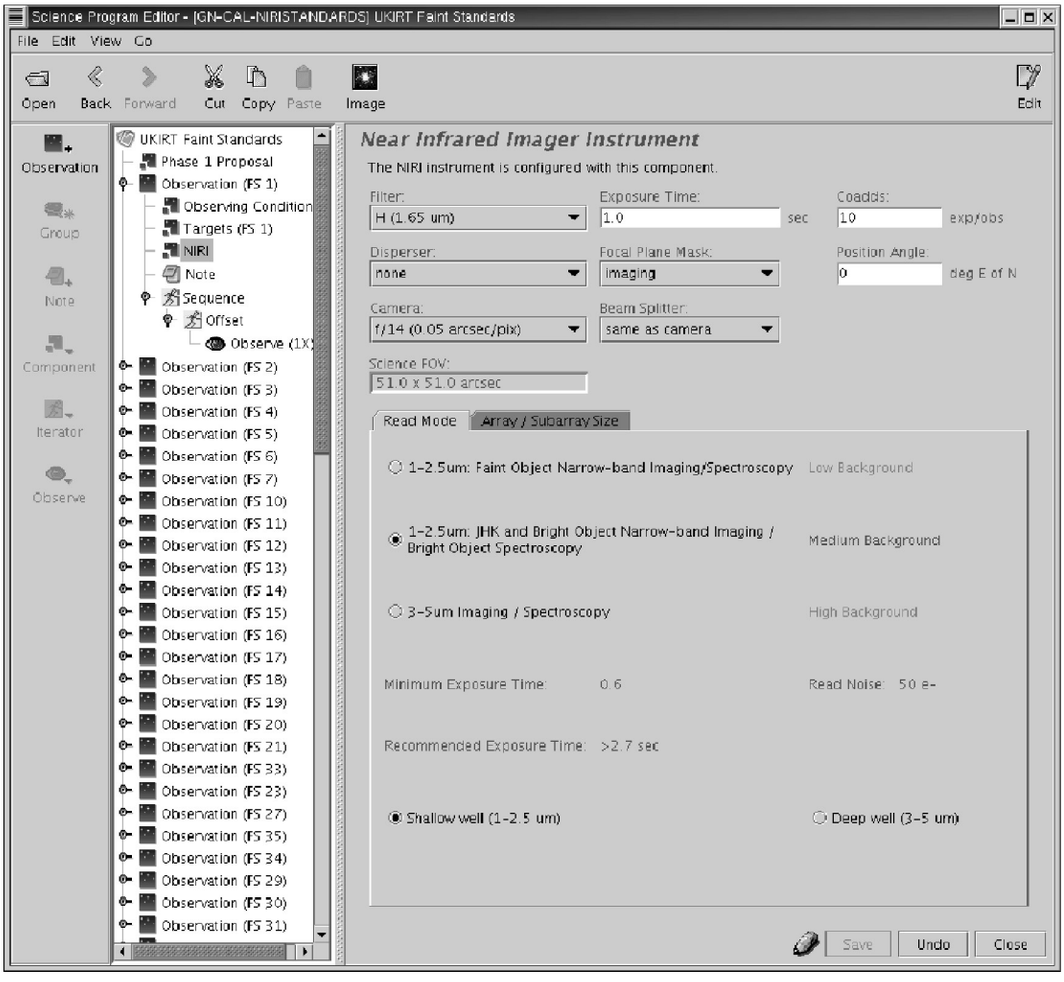

FIG. 12.—NIRI component in the OT. The OT is the primary tool for executing science observations at the telescope. It is also the tool used by astronomers to define their phase II programs.

the telescope (e.g., target and offset coordinates, guiding information), calibration unit (flats, darks, and arc lamp spectra), and instrument (filter selection, exposure time, etc.). The OT allows for complex sequences of offset exposures, instrument configurations, and calibrations to be automatically and efficiently executed.

To make the OT interface to NIRI easily usable for astronomers who may not be familiar with the detailed workings of the instrument, the NIRI component in the OT includes only a few specific possible configurations. The NIRI software interprets the OT configurations and moves the three filter wheels, focus stage, focal plane mask wheel, and camera optics appropriately. Logic is included in the software to prevent flooding of the detector with thermal photons during changes. The NIRI software also sets a number of detector controller parameters for the observing mode selected. These modes include thermal IR imaging, wide-field imaging, low-background imaging, and spectroscopy. Two additional modes, polarimetry and coronagraphic imaging, have not yet been commissioned. The NIRI components and array readout modes available through the OT interface are shown in Figure 12. Expected read noise and minimum recommended exposure times are listed for the mode selected. A subarray of the NIRI ALADDIN detector can be read out if shorter integrations are required.

Figure 13 shows an image of the young stellar object AFGL 2591 obtained with the f/6 wide-field camera of NIRI. The data were taken in the *J*, *H*, and *K* filters in the usual dithering procedure. The on-chip integration time was 2 s, and at each dither position, five such short integrations were co-added to obtain an image with higher dynamic range. In the *J* band, 12 such co-added exposures were taken, while in the *H* and *K* bands, six exposures were obtained. The data are presented as a false-color image with *J* coded as blue, *H* as green, and *K* as red.

FIG. 13.—False-color *J*, *H*, *K* color image of the young outflow object AFGL 2591. The image was taken with the f/6 wide-field mode of NIRI (Gemini Observatory/ Colin Aspin).

9. COMMUNITY USE OF NIRI

Community access to NIRI was first offered in 2001. During the first year, most NIRI observations were canceled so that we could address the instability problem in the camera steering mirrors. We also lost a significant fraction of the scheduled observing time to bad weather during the winter of 2001–2002. Nevertheless, data were collected for 15 programs in the 2002A queue. Early in semester 2002B, the bearing in the pupil wheel seized, compromising queue observations for a couple of months. After repair of the pupil wheel bearing, data were collected for a number of programs later in the semester. During early 2003 we focused on imaging programs because of recurring unreliability of the pupil wheel motor, which would have made the frequent use of the grisms risky. Observations for 15 programs were made in 2003A, and almost all the band 1 (highest rank) programs were completed. After some repair and maintenance work in summer of 2003, all mechanisms are now functioning properly. Semester 2003B is now underway, and excellent data in both imaging and spectroscopic modes have been collected. A review of the progress during each semester can be found in the archives of the "Hot News" updates on the NIRI Web pages.[6]

One of the first successful science observations with NIRI in 2001 was a highly ranked proposal to measure the brightness of a very distant Type Ia supernova at 1.2 and 2.1 μm. The observation of SN 2001 HB consisted of 5 hr total integration in each of the J and K' (Wainscoat & Cowie 1992) filters with median image quality of 0.″5 FWHM. The data were collected as part of the NIRI "system verification" program and released to the community. System verification data was used to test the reduction software and to familiarize observers with NIRI data in advance of an observing run.

Over the past 2 years, an increasingly diverse group of science observations have been completed. Imaging with the wide-field f/6 camera accounts for approximately 70% of all observations; most of the remainder has been spectroscopy, with a small fraction of the time being used for *L*- and *M*-band imaging with the finer plate scales. The wide-field imaging mode has been very useful for studying the metal dependence of Cepheid luminosities in the nearby spiral galaxy M33 and the properties of stars in the metal-rich open cluster NGC 6791. The excellent spatial resolution also makes NIRI ideal for studying the properties of very distant star-forming galaxies discovered using submillimeter observations at wavelengths where extinction by dust is minimized. NIRI has also been used to search for planets circling white dwarfs and for "weather" variations on rotating brown dwarfs. Another current NIRI program hopes to take advantage of massive Abell clusters to gravitationally magnify the faint light coming from distant galaxies at redshifts approaching $z \sim 7$; at such large redshifts, we can only hope to detect their light in the near-IR. NIRI has also been used to image the host galaxies of high-redshift ($z \sim 5$) quasars (Hutchings 2003).

NIRI's spectroscopic mode has also produced some excellent results. In one of the first trials of nonsidereal tracking with Gemini, we successfully measured the spectra of distant asteroids orbiting in the Lagrange points of Saturn. More recently, NIRI was used to take spectra of Charon and even fainter, more elusive Kuiper Belt objects. Farther from home, spectra for the most distant radio galaxies known have been collected using NIRI. At thermal wavelengths, NIRI spectra of brown dwarfs have provided insight into the molecular chemistry of substellar objects.

NIRI has been used extensively by both classically scheduled visiting observers and by staff astronomers executing queued observations. In the first semesters, the emphasis was on queue observations, since queue scheduling allows more flexibility in dealing with telescope or instrument problems. The high-level software needed to support classical observers has also been improving slowly through the years. The flexibility of the queue allowed us to respond to an opportunity in 2002 to observe the IR afterglow of an X-ray–bursting magnetar. The NIRI observations clearly showed the connection of the disruption of the neutron star crust, which generates X-rays, to the surrounding gas, from which the IR emission arises (Kaspi et al. 2003). In the coming semester, we plan to accept proposals to observe similar targets of opportunity and quick response observations as part of the regular NIRI queue.

[6] http://www.gemini.edu/sciops/instruments/niri/NIRIIndex.html.

The NIRI project was funded by the National Science Foundation and the University of Hawaii. We wish to thank the IfA directors Donald N. B. Hall, Robert McLaren, and Rolf-Peter Kudritzki for their steady support throughout this project.

The NIRI project has involved many individuals over many years. We wish to acknowledge the contributions by J. E. Graves, working on the installation of the optics, by our administrative officer, Gale Yamada, our secretary, Jill Kajikawa-Kent, and the IfA engineers Tony Young, Jeff Douglass, Jim Bell, and Doug Neill, as well as technicians Kelley Collins, Paul Uemura, and Freddie Reduta. We appreciate the help by Mark Trueblood, who managed the NIRI contract at the US Gemini Project Office. Dave Montgomery assisted us in resolving the problems with the beam-steerer bearings. The commissioning of NIRI at the Gemini telescope was supported by Ian Richardson, Corinne Boyer, Tom Geballe, Colin Aspin, Dolores Walther, and Scott Fisher.

The Gemini Observatory is operated by the Association of Universities for Research in Astronomy, Inc., under a cooperative agreement with the NSF on behalf of the Gemini partnership: the National Science Foundation (United States), the Particle Physics and Astronomy Research Council (United Kingdom), the National Research Council (Canada), CONICYT (Chile), the Australian Research Council (Australia), CNPq (Brazil), and CONICET (Argentina).

REFERENCES

Bell, J., Douglass, J., Hodapp, K.-W., Robertson, L., Tokunaga, A. T., & Young, T. T. 1998, Proc. SPIE, 3354, 1103
Douglass, J., Young, T. T., Hodapp, K.-W., Yamada, H., & Robertson, L. 1998, Proc. SPIE, 3354, 1062
Fowler, A. M., Bass, D., Heynssens, J., Gatley, I., Vrba, F. Ables, D., Hoffman, A., Smith, M., & Woolaway, J. 1994, Proc. SPIE, 2268, 340
Fowler, A. M., Gatley, I., McIntyre, P., Vrba, F. J., & Hoffman, A. W. 1996, Proc. SPIE, 2816, 150
Glasse, A. C., Atad-Ettedgui, E. I., & Harris, J. W. 1997, Proc. SPIE, 2871, 1197
Hodapp, K.-W., Hora, J., Graves, E., Irwin, E., Yamada, H., Douglass, J., Young, T. T., & Robertson, L. 2000, Proc. SPIE, 4008, 1334
Hodapp, K.-W., et al. 1996, NewA, 1, 177
———. 1998, Proc. SPIE, 3354, 545
———. 2003, Proc. SPIE, 4841, 869
Hora, J. L., Hodapp, K.-W., Irwin, E. M., Keller, T. J., & Young, T. T. 1995, Proc. SPIE, 2475, 308
Hutchings, J. B. 2003, AJ, 125, 1053
Kaspi, V. M., Gavriil, F. P., Woods, P. M., Jensen, J. B., Roberts, M. S. E., & Chakrabarty, D. 2003, ApJ, 588, L93
Saddlemyer, L. K., Herriot, G., & Veran, J.-P. 2000, Proc. SPIE, 4007, 649
Thornton, R., Young, T. T., Hodapp, K.-W., Douglass, J., & Yamada, H. 1998, Proc. SPIE, 3354, 1077
Tokunaga, A. T., Simons, D. A., & Vacca, W. D. 2002, PASP, 114, 180
Toomey, D. W., Stahlberger, W., & Watanabe, D. 1994, Proc. SPIE, 2198, 650
Wainscoat, R. J., & Cowie, L. L. 1992, AJ, 103, 332
Young, T. T., Hodapp, K.-W., Douglass, J., Neill, D., Irwin, E., & Robertson, L. 1998, Proc. SPIE, 3354, 1084